O−H···O versus O−H···S Hydrogen Bonding I: Experimental and Computational Studies on the *p*-Cresol·H_2O and *p*-Cresol·H_2S Complexes

Himansu S. Biswal,[†] Pranav R. Shirhatti,[‡] and Sanjay Wategaonkar*

Department of Chemical Sciences, Tata Institute of Fundamental Research, Homi Bhabha Road, Colaba, Mumbai 400 005, India

Received: February 2, 2009; Revised Manuscript Received: March 8, 2009

The weak hydrogen bonding ability of sulfur-containing hydrides makes it difficult to study their complexes and has not been characterized experimentally so far. In this work, the hydrogen-bonded complexes of H_2S and H_2O with *p*-cresol (*p*-CR) were studied using a variety of techniques such as two-color resonant two-photon ionization (2c-R2PI) spectroscopy, single vibronic level fluorescence (SVLF) spectroscopy, resonance ion dip infrared spectroscopy (RIDIRS), and fluorescence dip infrared spectroscopy (FDIRS), with an aim of comparing the nature and strength of their respective hydrogen bonding abilities. The intermolecular stretch (σ) and the shift in the O−H stretching frequency of *p*-CR in the complex were taken as the measures of the O−H···O and O−H···S hydrogen bonding strength. The experiments were complemented by the *ab initio* calculations, atoms in molecules (AIM), natural bond orbital (NBO), and energy decomposition analyses carried out at different levels of theory. The experimental data indicates that in the *p*-CR·H_2S complex, the phenolic OH group acts as a hydrogen bond donor, and sulfur as the acceptor. Further, it indicates that the *p*-CR·H_2S complex was about half as strong as the *p*-CR·H_2O complex. The AIM and NBO analyses corroborate the experimental findings. The energy decomposition analyses for the O−H···S hydrogen bond in the *p*-CR·H_2S complex reveal that the dispersion interaction energy has the largest contribution to the total interaction energy, which is significantly higher than that in the case of the *p*-CR·H_2O complex.

1. Introduction

Noncovalent interactions such as van der Waals and hydrogen bonding have been a thrust area of research in recent years. With the advances in the experimental techniques and computational resources, a variety of different hydrogen bonding interactions have been reported in the literature in recent times.[1] It is the most common and yet an important type of interaction which is encountered in many chemical and biological processes. It plays a vital role in defining the crystal packing of many organic and organometallic molecules, in regulating 3D structure and controlling the functions of biological molecules, as well as modulating the reactivity of different groups within a molecule. Owing to its importance, a lot of effort has been put into understanding its nature, and by now, the hydrogen bonding between X−H···Y, where X and Y are two electronegative atoms, is fairly well understood. In the classical electrostatic model, significant charge transfer occurs from the acceptor Y to the donor or, more precisely, from the lone pair orbital on Y to the σ^*_{X-H} antibonding orbital, resulting in weakening of the X−H bond with concomitant elongation[2] of the XH bond length. This elongation of the X−H bond manifests in a decrease in the X−H stretching frequency, and such a frequency red shift with respect to that of the free monomer has been regularly used as a fingerprint of hydrogen-bonded complex.

Sulfur is the least electronegative element compared to N, O, and F (2.58 for S, 3.04 for N, 3.44 for O, 3.98 for F on the Pauling scale).[3] Further, due to the very small difference in the electronegativity of H and S ($\Delta \sim 0.38$ on the Pauling scale) and poorer match between the hard proton (hard acid) and soft sulfur (soft base), intrinsically, it is not a good hydrogen bond (HB) acceptor. Sulfur also happens to be a biologically abundant element (amino acids, disulfide bridges, etc.), and the existence of the X−H···S (X = N, O) HB is well established from the crystallographic data on proteins and organic molecules.[4−15] Despite this, the experimental investigations have been very scant on the X−H···S hydrogen-bonded systems. A large number of computational studies have been devoted, however, to investigate either the H−S···π or S−H···π interaction in the case of H_2S and aromatic hydrocarbon complexes.[15−25] The authors' first report on the experimental observation of O−H···S HB in simple model compounds of two naturally occurring amino acids, tyrosine and methionine (*p*-CResol was taken for tyrosine and dimethyl sulfide (DMS) for methionine),[26] indicated that the O−H stretch red shift in these systems was almost the same as that for the O−H···O HB in the case of the *p*-cresol-$(H_2O)_1$ complex. However, it was felt that this comparison would not be appropriate as the sulfur bound to two methyl groups in DMS would not be the same HB acceptor as that in the case of H_2S.

The historic Pauling definition of HB states that "for the X−H···Y hydrogen bond, both X and Y atoms should be electronegative, the X···Y distance should be shorter than the corresponding sum of van der Waals radii, and this interaction is mostly electrostatic in nature".[27] Although the electrostatic origin accounts for the major part of the HB strength, there are other interactions which could also contribute to the strength of HBs. Very recently, Desiraju claimed that "the hydrogen bond is not a simple interaction but a complex conglomerate of at least four component interaction types, electrostatic (acid/base), polarization (hard/soft), van der Waals (dispersion/repulsion), and covalency (charge transfer)".[28] The relative extent of each

---

* To whom correspondence should be addressed. Phone: 91-22-2278-2259. Fax: 91-22-2278-2106. E-mail: sanwat@tifr.res.in.

[†] E-mail: himansu@tifr.res.in.

[‡] E-mail: pranav@tifr.res.in.

10.1021/jp9009355 CCC: $40.75

of these interactions determines the strength of the HB and its other characteristics such as directionality, the shift in the X−H stretching frequency, and so forth. In this context, it is worth investigating the nature of the O−H···S hydrogen bonding and comparing it with the conventional O−H···O hydrogen bond. Therefore, the purpose of current study is to compare the nature of the O−H···S with the O−H···O hydrogen bonding in the p-CR·H_2O and p-CR·H_2S complexes. This is a first of the series of XH···SR_2 (X = O,N; R = radical) HB investigations that we have been carrying out in our laboratory. The experiments were carried out in the gas phase under supersonic jet conditions. Different computational methods have been used to quantify these interactions and to aid the experimental findings.

In regard to the comparison between the O−H···O and O−H···S interactions in gas phase, there has been only one report in the literature where both computational and experimental methods have been utilized to study the nature of the HB.[29] D. L. Howard and H. G. Kjaergaard have claimed that sulfur is nearly equivalent to oxygen as a hydrogen bond acceptor from the vapor-phase infrared spectroscopic study of the complexes of methanol with dimethylether and dimethylsulfide. However, because of very weak absorbance due to the dimethylsulfide−methanol complex in the spectrum and broad IR spectra, it was difficult to obtain precise information about the O−H frequency shifts in these complexes. Therefore, it is essential to look at such a type of interaction using the supersonic jet expansion technique, which offers better precision.

2. Experimental Details

The experimental setup, the details of which have been described elsewhere,[30] consisted of two 10 in. diameter differentially pumped stainless steel chambers. A 300 μm pulsed nozzle (General Valve, series 9) housed in the first chamber was used to generate a cold beam of molecules, which was collimated using a skimmer located ~25 mm downstream from the nozzle orifice. The collimated beam entered the time-of-flight mass spectrometer (TOFMS) with a 50 cm flight tube and a 25 mm diameter channeltron multiplier (Dr. Sjuts Optotechnik GmbH; KBL25RS) detector housed in the second chamber. The output of the channeltron was sent to a digitizing storage oscilloscope (LeCroy 9450) interfaced to a PC through a preamplifier (ORTEC, Model VT120). For the REMPI experiments (two-color, two-photon), a 10 Hz, nanosecond Nd^{3+}:YAG (Quantel Brilliant)-pumped dye laser (Molectron DL18P) was used to provide the fixed D_0-S_1 ionization source, and another Nd^{3+}:YAG (Quantel YG781C) laser-pumped dye laser (Quantel TDL70) was used to provide the tunable S_1-S_0 excitation source. The two copropagating beams were spatially and temporally overlapped and were focused onto the molecular beam using a 50 cm focal length lens. Typical pulse energies were ~5−10 μJ for the excitation laser and ~100 μJ for the ionization laser. The dye lasers were calibrated by means of the optogalvanic method using an Fe−Ne hollow cathode lamp. The single vibronic level fluorescence (SVLF) spectroscopy was carried out using a PMT (Hamamatsu R943)/monochromator (McPherson Inc., Model 2035) assembly. The slit width was typically set at 100−20 μm, corresponding to a band pass of 15 cm^{-1}.

Resonance ion dip infrared spectroscopy (RIDIRS) was used to record the IR spectra of the p-CR and its complexes. In this technique, the S_1-S_0 electronic excitation laser is tuned to the band origin transition of a particular species, and the ionization laser is set a little above the D_0-S_1 transition, which gives the ion signal proportional to the ground-state population of the species in the beam. The tunable IR laser is introduced 50−100 ns prior to the UV laser pulses. Whenever the IR laser is resonant with the vibrational transition of the species being probed, it depletes the population of the species in the ground state. The infrared resonances were detected as the dips in the ion signal because of the population depletion. The tunable IR source was a 5−6 ns, 10 Hz seeded Nd^{3+}:YAG laser (Quanta-Ray PRO Series, PRO 230-10)-pumped dye laser (Sirah, CSTR LG 18 532). The dye laser output was mixed with the 1064 nm output of the Nd^{3+}:YAG laser in a $LiNbO_3$ crystal to generate the IR output by the difference frequency generation technique. The O−H stretching region (3750−3300 cm^{-1}) was covered using styryl-8 dye (Exciton, Inc.). All three lasers were temporally synchronized by a master controller (SRS DG-535). For probing the OH stretch in the S_1 state of the complexes, fluorescence dip infrared spectroscopy (FDIRS) was used. The FDIRS technique is pretty similar to the RIDIRS, except that one probes the S_1-S_0 fluorescence intensity instead of the ion signal. In the case of the excited-state FDIRS, the IR pulse is introduced a little after the UV excitation pulse, and the IR resonances in the S_1 state are probed by monitoring the fluorescence intensity. The time delay between UV and IR pulses must necessarily be kept shorter than the excited-state lifetime. In our case, the typical delay between the UV and IR laser was ~5 ns.

The reagent p-CR was purchased from Sigma-Aldrich and used without further purification. The sample was heated to about 50−60 °C to generate sufficient vapor pressure to record the spectra with a good S/N ratio. Helium obtained from local commercial sources was used without further purification as the buffer gas. The buffer gas was flowed over a reagent bottle containing H_2O to synthesize the p-CR·H_2O complexes. The optimum amount of H_2O vapor required for generating the 1:1 complex was maintained by means of a needle valve. A 2−5% premix of H_2S in helium was used to generate a 1:1 complex of p-CR and H_2S. The typical backing pressure employed during the experiments was 2.5−3 atm. The typical working pressure in the source chamber was $\sim 6 \times 10^{-5}$ Torr, and in the TOFMS chamber, it was $\sim 2 \times 10^{-6}$ Torr.

3. Computational Details

The geometrical parameters of the p-CR·H_2O and p-CR·H_2S complexes and the free monomer were fully optimized at the MP2/aug-cc-pVDZ, B3LYP/aug-cc-pVDZ, and MPWB1K/aug-cc-p-VDZ levels of theory. The equilibrium structures were examined by the harmonic vibrational frequency calculations at all levels of theory. Three different levels of theory have been chosen for different reasons; MP2 takes care of the electron correlation,[31,32] which is important for the weak interactions, while DFT/B3LYP is computationally less expensive and gives somewhat reliable harmonic vibrational frequencies.[33] It has been recently shown that the DFT computations using the MPWB1K functional give the interaction energies which are comparable with the CCSD(T) level of calculation, and these can be computed within a relatively short computational time.[24,25,34,35] The interaction energies for all of the complexes were calculated after applying the zero-point energy (ZPE), the basis set superposition error (BSSE), and the fragment relaxation energy corrections to the total binding energy. The excited-state geometry optimizations and the frequency calculations for both monomers and complexes were done at the CIS/aug-cc-pVDZ level of theory. All of the calculations were carried out using the Gaussian03 program suite.[36] The three-dimensional pictures of the complexes were generated using the ChemCraft graphics program (trial version).[37]

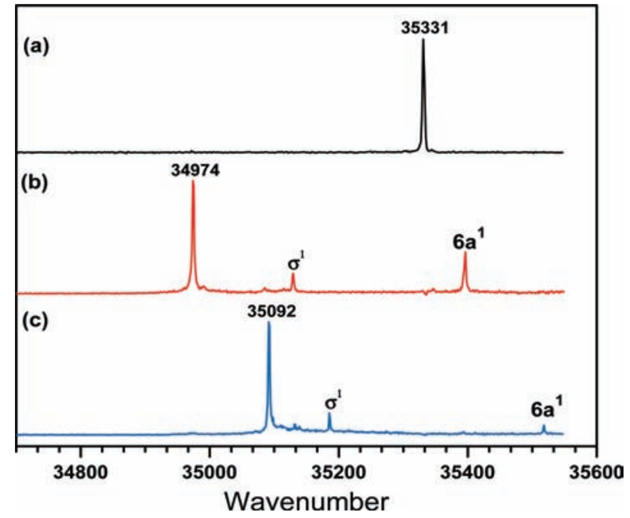

Figure 1. Two-color R2PI spectra of (a) *p*-CR, (b) *p*-CR·H_2O, and (c) *p*-CR·H_2S.

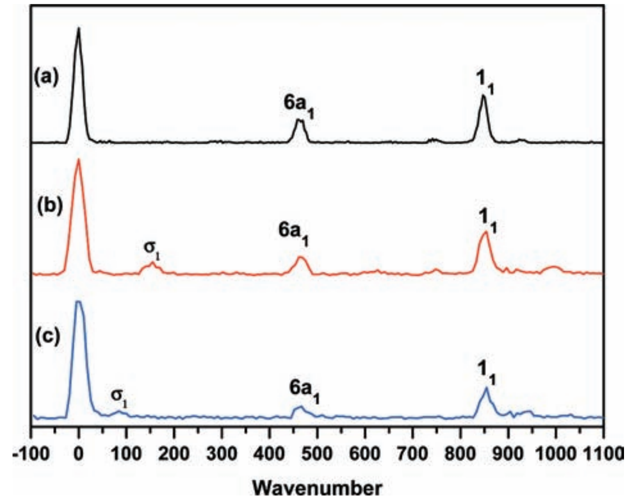

Figure 2. SVLF spectra of (a) *p*-CR, (b) *p*-CR·H_2O, and (c) *p*-CR·H_2S band origin excitations.

The theory of atoms in molecules (AIM)[38−40] was used to investigate the electronic densities and the intermolecular hydrogen bonding interactions. The topological properties of electron densities for the monomers and complexes at the bond critical points (BCPs) were calculated using the AIM2000 program.[41] The wave functions computed at the aforementioned three levels of theory were used to calculate the electron density $\rho(r)$ and Laplacian $\nabla^2\rho(r)$ at the bond critical points and the integrated properties like atomic charge $q(H)$, atomic polarization moment $M(H)$, atomic volume $v(H)$, and atomic energy $E(H)$ in the atomic basin of hydrogen. To evaluate the direction and magnitude of the donor−acceptor interactions, the natural bond orbital (NBO)[42−44] analysis for all of the complexes was performed using the NBO 5.0 program.[45]

The interaction energies of the complexes were decomposed into physically meaningful individual energy components[46] at the HF/aug-cc-pvDZ level of theory using the natural energy decomposition analysis (NEDA)[47−49] and the Kitaura and Morokuma (KM)[50] and reduced variational space self-consistent field (RVS)[51] decomposition analyses. The KM and RVS decomposition analyses were performed using the Gordon and Chen[52] algorithm in the GAMESS, U.S.A.[53] NEDA calculations were performed with the NBO 5.0 program[43,45] linked to the GAMESS package.

4. Experimental Results

Figure 1 shows the two-color R2PI spectra of *p*-CR (Figure 1a), *p*-CR·H_2O (Figure 1b), and *p*-CR·H_2S (Figure 1c). In all cases, the ionization laser energy was at 30770 cm^{-1}, that is, just above the D_0−S_1 transition of *p*-CR.[54] The band origins of *p*-CR, *p*-CR·H_2O, and *p*-CR·H_2S were observed at 35331, 34974, and 35092 cm^{-1}, respectively. The spectral features and the observed band origins for *p*-CR and *p*-CR·H_2O are in good agreement with those reported in the literature.[54−59] The red shift in the band origin of the *p*-CR·H_2O complex was 357 cm^{-1}, whereas that of the *p*-CR·H_2S complex was 239 cm^{-1}. Incidentally, the band origin red shift in the *p*-CR·H_2O complex is comparable to that reported for the phenol·H_2O complex, namely, 356 cm^{-1}. The transitions at 155 and 422 cm^{-1} in Figure 1b and at 93 and 426 cm^{-1} in Figure 1c were assigned as the intermolecular stretch (σ^1) and intramolecular 6a^1 transitions of the *p*-CR·H_2O and *p*-CR·H_2S complexes, respectively. To obtain the ground-state spectral information, especially the value of the intermolecular stretch, σ, the SVLF spectra were recorded for both the monomer and the complexes by exciting at their respective band origins.

Figure 2 shows the SVLF spectra from the band origin excitations of *p*-CR (Figure 2a), *p*-CR·H_2O (Figure 2b), and *p*-CR·H_2S (Figure 2c) up to 1100 cm^{-1} from the resonance transition. Apart from the most active modes such as the 6a and mode 1, transitions were observed at 148 and 85 cm^{-1}, corresponding to the intermolecular stretch for the *p*-CR·H_2O and *p*-CR·H_2S complexes, respectively. The prominent spectral features observed in the S_0 and S_1 states for the monomers and the complexes are provided in Table 1. To assign the aromatic ring vibrations, Varsanyi's nomenclature[60] for the benzene ring modes was adopted. The σ^1 and σ_1 for *p*-CR·H_2O are 155 and 148 cm^{-1}, respectively, while those for *p*-CR·H_2S are 93 and 85 cm^{-1}, respectively. The greater intermolecular stretching frequencies in the excited S_1 state (σ^1) relative to those in the ground S_0 state (σ_1) for both of the complexes suggest that the hydrogen bonding is stronger in the excited S_1 state for both of the complexes.

The RIDIRS spectra of *p*-CR, *p*-CR·H_2O, and *p*-CR·H_2S are shown in Figure 3. The wavelength region between 3300 and 3700 cm^{-1} was scanned while monitoring the ion signal due to the monomer and the complexes. In all of the cases, the UV laser (probe laser) was fixed at the respective band origin while the IR laser (pump laser) was scanned; the time delay between

TABLE 1: Ground-State (S_0) and Excited-State (S_1) Vibrational Frequencies (cm^{-1}) for *p*-CR, *p*-CR·H_2O, and *p*-CR·H_2S

	modes								
molecules	BO	σ_1	σ^1	6a$_1$	6a^1	1$_1$	1^1	ν_1(O−H)	ν^1(O−H)
p-CR	35331			458	419[a]	847	806[a]	3658	3581[c]
p-CR·H_2O	34974	148	155	461	422	854	810[b]	3531	3393
p-CR·H_2S	35092	85	93	467	426	855		3556	3429

[a] Reference 54. [b] Reference 56. [c] Reference 62.

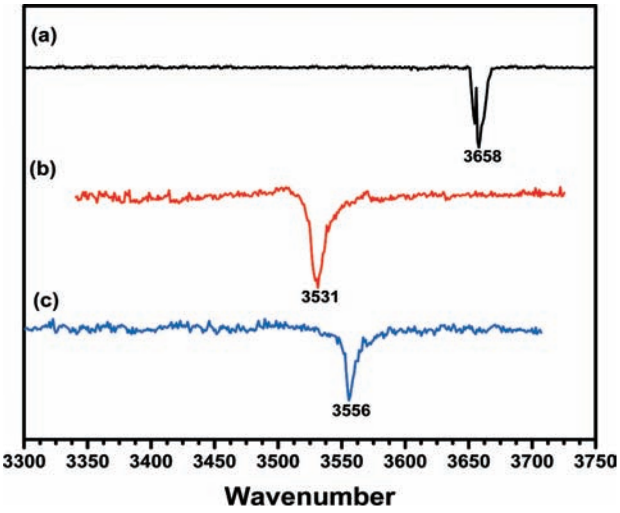

Figure 3. RIDIRS spectra of the S_0 state of (a) *p*-CR, (b) *p*-CR$\cdot$$H_2O$, and (c) *p*-CR$\cdot$$H_2S$ recorded while tuning the probe laser at the band origin of the respective species.

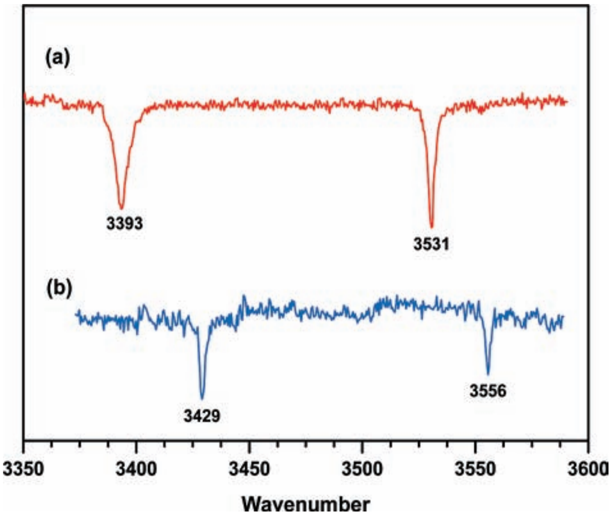

Figure 4. FDIR spectra of the S_1 state of (a) *p*-CR$\cdot$$H_2O$ and (b) *p*-CR$\cdot$$H_2S$ recorded while tuning the probe laser at the band origin of the respective species. The pump laser was introduced ∼5 ns after the probe laser.

the IR laser and the UV laser was ∼50 ns, with the IR laser arriving ahead of the UV laser. The OH stretch frequency of the *p*-CR in the ground S_0 state was found to be 3658 cm^{-1}, which is in excellent agreement with the literature value.[59] The OH stretching frequencies of the *p*-CR$\cdot$$H_2O$ and *p*-CR$\cdot$$H_2S$ complexes were observed at 3531 and 3556 cm^{-1}, respectively. This gives the OH stretch red shift of 127 cm^{-1} in the case of *p*-CR$\cdot$$H_2O$ and 102 cm^{-1} for the *p*-CR$\cdot$$H_2S$. This trend in the OH stretch red shift correlates well with the intermolecular stretch frequencies (σ) mentioned above.

The FDIRS was used to determine the excited-state OH stretching frequencies in the complexes. In this case, the IR laser was introduced just after (∼5 ns) the probe laser. The delay between the pump and probe was so adjusted that the ground-state FDIR and excited-state FDIR could be observed together. Figure 4 shows the excited-state FDIR spectra of the *p*-CR$\cdot$$H_2O$ and *p*-CR$\cdot$$H_2S$ complexes. The excited-state OH stretching frequencies for the *p*-CR$\cdot$$H_2O$ and *p*-CR$\cdot$$H_2S$ complexes were observed at 3393 and 3429 cm^{-1}, respectively. In the case of the monomer, the excited-state OH stretch could not be observed due to very short fluorescence lifetime of *p*-CR. Therefore, the excited-state OH stretching frequencies of the *p*-CR$\cdot$$H_2O$ and *p*-CR$\cdot$$H_2S$ complexes were compared with the excited-state OH stretch of phenol[61,62] (at 3581 cm^{-1}), which has close structural similarity with *p*-CR, and the ground-state OH stretch of phenol and *p*-CR are almost same.[59,62−64] The OH stretch red shifts relative to that of the monomer were much greater in the excited state than those in the ground state for both complexes. For the *p*-CR$\cdot$$H_2O$ complex, it was 188 cm^{-1}, and that for the *p*-CR$\cdot$$H_2S$ complex was 152 cm^{-1}; these can be compared with their ground-state values of 127 and 102 cm^{-1}, respectively. Hence, it can be inferred that both H_2O and H_2S form stronger complexes in the excited state relative to those in the ground state. For both the *p*-CR$\cdot$$H_2O$ and *p*-CR$\cdot$$H_2S$ complexes, the OH stretches in the excited state were red shifted from their respective ground-state fundamental frequencies by 138 and 127 cm^{-1}, respectively, and the line widths of the excited-state OH stretches were almost two times those of the ground-state transitions, indicating an increase in the IR transition probability and hence the hydrogen bonding strength in the excited state.

In summary, H_2O and H_2S complexes show similar spectral features in the two-color R2PI, SVLF, RIDIRS, and excited-state FDIR spectra, reflecting that the O−H···S hydrogen bonding is similar to the O−H···O hydrogen bonding, albeit the O−H···S hydrogen bonding is weaker than the O−H···O hydrogen bonding.

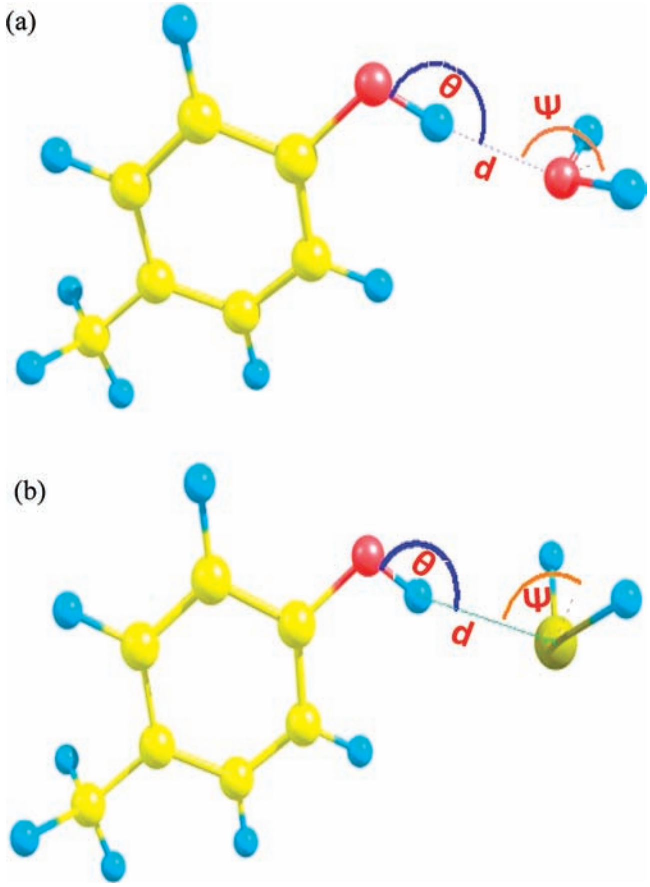

Figure 5. The optimized structures of (a) *p*-CR$\cdot$$H_2O$ and (b) *p*-CR$\cdot$$H_2S$ obtained at MP2/aug-cc-pVDZ level of theory.

5. Computational Results

5.1. Equilibrium Geometry and Interaction Energy. Figure 5 shows the structures of the *p*-CR$\cdot$$H_2O$ (Figure 5a) and *p*-CR$\cdot$$H_2S$ (Figure 5b) complexes optimized at the MP2/aug-cc-pVDZ level of theory. All of the geometrical parameters such

TABLE 2: Geometrical Parameters (Å and degrees) Computed at Different Levels of Theory

geometrical parameters	MP2/aug-cc-pVDZ		MPWB1K/aug-cc-pVDZ		B3LYP/aug-cc-pVDZ	
	p-CR·H_2O	p-CR·H_2S	p-CR·H_2O	p-CR·H_2S	p-CR·H_2O	p-CR·H_2S
$d_{H\cdots Y}$ (Å)[a]	1.872	2.437	1.880	2.512	1.888	2.520
$R_{O\cdots Y}$ (Å)[a]	2.848	3.404	2.839	3.463	2.858	3.463
Δr_{O-H} (Å)	0.009	0.006	0.009	0.006	0.009	0.006
θ (deg)	176.9	172.1	173.8	171.0	173.1	163.9
Ψ (deg)	134.3	92.4	134.8	94.5	134.1	91.6

[a] Y: O or S.

TABLE 3: Calculated Binding Energies and Different Correction Terms (kcal/mol) for p-CR·H_2O and p-CR·H_2S Complexes

energy components (kcal/mol)	MP2/aug-cc-pVDZ		MPWB1K/aug-cc-pVDZ		B3LYP/aug-cc-pVDZ	
	p-CR·H_2O	p-CR·H_2S	p-CR·H_2O	p-CR·H_2S	p-CR·H_2O	p-CR·H_2S
ΔE_{BE}	−7.52	−5.28	−6.36	−3.59	−5.88	−3.01
ΔE_{BSSE}	1.39	1.60	0.33	0.50	0.30	0.24
ΔE_{Relax}	0.09	0.04	0.09	0.03	0.10	0.06
ΔE_{BE}^{BSSE}	−6.12	−3.68	−6.03	−3.09	−5.59	−2.78
ΔZPE	1.75	1.15	1.68	1.26	1.63	1.11
$\Delta E_{BE}^{BSSE+Relax+ZPE}$	−4.29	−2.49	−4.26	−1.80	−3.86	−1.61

as the $d_{H\cdots Y}$ (Y = O or S), $R_{O\cdots Y}$, Δr_{OH}, the H bond angle θ (i.e., ∠OHY), and the angle (Ψ) made by the C_2 axis of the H_2Y with the OH···Y are listed in Table 2. For the H_2O complex, the hydrogen bond angle (θ) was ~174° at all levels of theory, where asfor the H_2S complex, it was ~171° at the MP2 and DFT(MPW1BK) levels, and it was 164° at the B3LYP level of theory. The increase in the O−H bond length in the p-CR·H_2O complex was higher than that in the p-CR·H_2S complex. These geometrical parameters are in good agreement with those reported for the methanol−dimethylsulfide and methanol−dimethylether complexes.[29] The only parameter that differed was the hydrogen bond angles (θ),[29,65] which were ~165 and ~155° for the O−H···O and O−H···S H-bonded complexes, respectively.

The interaction energies for the complexes calculated at the above-mentioned three levels of theory are provided in Table 3. The first row of Table 3 lists the uncorrected binding energy (ΔE_{BE}), which was taken as the difference between the energy of the complex and that of the monomers. Different energy corrections like basis set superposition error (ΔE_{BSSE}), deformation or relaxation energy (ΔE_{elax}), and zero-point energy correction (ΔZPE) were applied to get the corrected interaction energy ($\Delta E_{BE}^{BSSE+Relax+ZPE}$). In Table 3, the subscripts to ΔE indicate the corresponding correction energy term, and superscripts indicate the energy corrections that were applied. The corrected binding energies of p-CR·H_2O and p-CR·H_2S are 4.29 and 2.49 kcal mol^{-1}, respectively, at the MP2 level. It may be noted that the corrected binding energy for the H_2O complex computed using the MPW1BK functional is in excellent agreement with the MP2 value; however, it is not quite so for the H_2S complex, where it was almost 25% less than that computed at the MP2 level and almost comparable to that for the B3LYP value.

Frequency calculations were carried out at all three different levels of theory for p-CR and its complexes with H_2O and H_2S and compared with the experimental observed frequencies. Table 4 lists the computed and experimentally observed O−H stretches (ν_{O-H}) for the ground S_0 state of the p-CR monomer and its complexes and the intermolecular stretch (σ) for the complexes. The computed frequencies were scaled by a factor of 0.966, which was obtained by minimizing the standard deviation. It can be seen that the OH stretching frequencies obtained at the MP2 and B3LYP levels are within 1% of the observed frequencies, whereas those computed using the MPWB1K functional are off by as much as 4−5%. However, the intermolecular stretching frequency computed at the MPWB1K

TABLE 4: Comparison of Computed Frequencies (cm^{-1}) at Three Different Levels of Theory and Experimentally Observed Frequencies

normal mode	MP2	MPWB1K	B3LYP	EXPT
ν_{O-H}(p-CR)	3679	3843	3688	3658
ν_{O-H}(p-CR·H_2O)	3510	3670	3503	3531
ν_{O-H}(p-CR·H_2S)	3550	3726	3555	3556
σ(p-CR·H_2O)	152	150	144	148
σ(p-CR·H_2S)	95	83	76	85

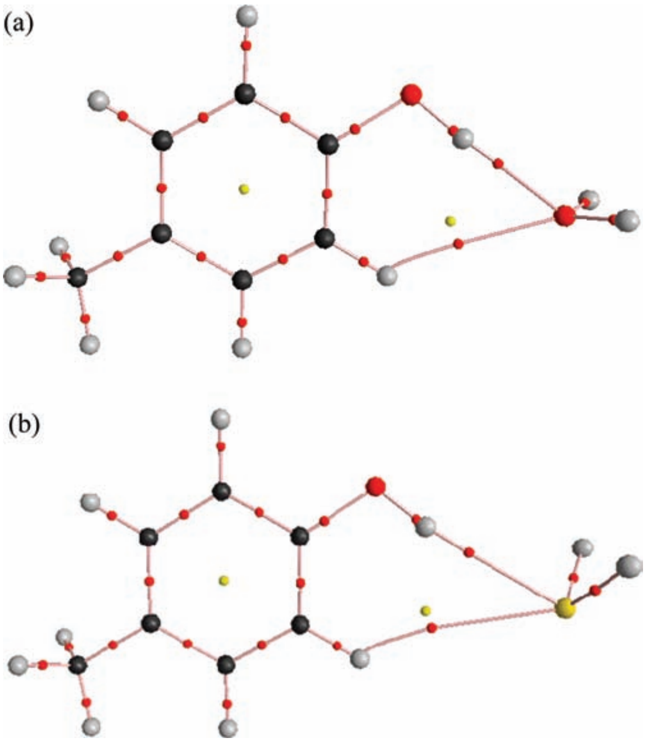

Figure 6. The molecular graphs of (a) p-CR·H_2O and (b) p-CR·H_2S, obtained using MP2/aug-cc-pVDZ wave function.

TABLE 5: AIM Parameters (au) for *p*-CR·H_2O and *p*-CR·H_2S Complexes Computed Using Three Different Levels of Theory

	MP2/aug-cc-pVDZ		MPWB1K/aug-cc-pVDZ		B3LYP/aug-cc-pVDZ	
AIM parameters	*p*-CR·H_2O	*p*-CR·H_2S	*p*-CR·H_2O	*p*-CR·H_2S	*p*-CR·H_2O	*p*-CR·H_2S
$\rho_{H\cdots Y}$[a]	0.0260	0.0160	0.0270	0.0144	0.0275	0.0148
$\nabla^2\rho_{H\cdots Y}$[a]	0.1134	0.0440	0.1051	0.0348	0.0975	0.0324
Δq_H	0.0540	0.0140	0.0399	0.0038	0.0345	−0.0012
ΔE_H	0.0299	0.0142	0.0234	0.0108	0.0185	0.0082
$\Delta\lvert M_H\rvert$	−0.0436	−0.0141	−0.0404	−0.0076	−0.0429	−0.0062
$\Delta\upsilon_H$	−8.8855	−4.4985	−8.4226	−3.1537	−8.6885	−2.7764
$R_{H\cdots BCP}$	0.63	0.76	0.64	0.81	0.65	0.83
$R_{Y\cdots BCP}$	1.24	1.68	1.24	1.70	1.24	1.69
$\langle R_{H\text{-}BCP}\rangle$[b]	0.78 ± 0.08					
$\langle R_{Y\text{-}BCP}\rangle$[b]	1.29 ± 0.07	1.76 ± 0.08				

[a] Y: O or S. [b] The values are taken from ref: 74.

TABLE 6: Summary of NBO Analyses ($E^{(2)}_{i\rightarrow j^*}$ is in kcal/mol, all other values are in au)

	MP2/aug-cc-pVDZ		MPWB1K/aug-cc-pVDZ		B3LYP/aug-cc-pVDZ	
NBO parameters	*p*-CR·H_2O	*p*-CR·H_2S	*p*-CR·H_2O	*p*-CR·H_2S	*p*-CR·H_2O	*p*-CR·H_2S
$\Delta q(H)$	0.0352	0.0133	0.0258	0.0062	0.0235	0.0053
$\Delta q(Y)$[a]	−0.0139	−0.0017	−0.0115	−0.0013	−0.0075	0.0006
$\delta(n_Y)$[a]	1.9801	1.9767	1.9745	1.9756	1.9724	1.9731
$\delta(\sigma^*_{O-H})$	0.0221	0.0244	0.0279	0.0259	0.0309	0.0291
$E^{(2)}_{i\rightarrow j^*}$	15.57	11.68	14.22	8.11	13.02	7.73
$\varepsilon^{(0)}_{j^*} - \varepsilon^{(0)}_{i}$	1.53	1.17	1.16	0.88	1.00	0.74
$\langle\varphi^{(0)}_i\lvert\hat{F}_{KS}\rvert\varphi^{(0)}_{j^*}\rangle$	0.14	0.10	0.12	0.08	0.10	0.07

[a] Y: O or S.

TABLE 7: Summary of Hybrids of O and S and the Coefficients for the σ_{O-H} and σ^*_{O-H} Orbitals

		MP2/aug-cc-pVDZ			MPW1BK/aug-cc-pVDZ			B3LYP/aug-cc-pVDZ		
			Coefficient			Coefficient			Coefficient	
molecules	orbital	Hybrid of O or S atom	O	H	Hybrid of O or S atom	O	H	Hybrid of O or S atom	O	H
H_2O	O(LP)	p			p			p		
H_2S	S(LP)	p			p			p		
p-CR	σ_{O-H}	$sp^{3.79}$	0.8652	0.5015	$sp^{3.72}$	0.8656	0.5007	$sp^{3.84}$	0.8649	0.5019
	σ^*_{O-H}	$sp^{3.79}$	0.5015	−0.8652	$sp^{3.72}$	0.5007	−0.8656	$sp^{3.84}$	0.5019	−0.8649
p-CR·H_2O	O(LP)	$sp^{2.02}$			$Sp^{2.17}$			$sp^{2.19}$		
	σ_{O-H}	$sp^{3.09}$	0.8799	0.4751	$sp^{3.05}$	0.8787	0.4774	$sp^{3.13}$	0.8776	0.4794
	σ^*_{O-H}	sp3.09	0.4751	−0.8799	$sp^{3.05}$	0.4774	−0.8787	$sp^{3.13}$	0.4794	−0.8776
p-CR·H_2S	S(LP)	$sp^{8.61}$			$sp^{12.20}$			$sp^{14.72}$		
	σ_{O-H}	$sp^{3.24}$	0.8743	0.4855	$sp^{3.25}$	0.8729	0.4879	$sp^{3.34}$	0.872	0.4895
	σ^*_{O-H}	$sp^{3.24}$	0.4855	−0.8743	$sp^{3.25}$	0.4879	−0.8729	$sp^{3.34}$	0.4895	−0.872

level was in the best agreement, perhaps fortuitously, with the observed value compared to those computed using the other two methods.

5.2. Atoms in Molecules (AIM) Study. AIM[38−40] calculations were done using the *ab initio* wave functions computed at the B3LYP, MPWB1K, and MP2 levels of theory for the monomers and the complexes. AIM theory takes electron density (ρ) as a starting point. The interaction between any two atoms in the system is characterized by the parameters associated with the electron density at the bond critical point (BCP) known as the (3,−1) critical point. The shortest gradient path connecting the two nuclei and the bond critical point represents a bond path. In terms of topological analysis of the electron density, these critical points and bond paths give rise to a molecular graph, which is a good representation of the bonding interactions or, in the present context, the hydrogen bonding interaction. Figure 6 shows the molecular graphs for *p*-CR·H_2O (Figure 6a) and *p*-CR·H_2S (Figure 6b) obtained using the wave functions computed at the MP2 level. The AIM criteria proposed by Popelier[66−68] that establish a classical hydrogen bond were applied for the O−H···O and O−H···S hydrogen-bonded complexes. These criteria are based on (1) the charge density [ρ_b] and the Laplacian of the charge density [$\nabla^2\rho_b$] determined at the bond critical points, (2) the topology of bond paths between the hydrogen atom and the hydrogen bond acceptor, (3) the mutual penetration of the hydrogen atom and an interacting bond, (4) the loss of charge and energetic destabilization of the hydrogen atom and the total charge that is transferred, (5) decrease of dipolar polarization of the hydrogen atom, and (6) decrease of the volume of the hydrogen. All of the topological parameters are listed in Table 5. Figure 6 shows the BCPs along the lines joining the OH and Y (Y = O, S) atoms for *p*-CR·H_2O (Figure 6a) and *p*-CR·H_2S (Figure 6b), respectively, which indicate the presence of a hydrogen bond between the *p*-CR and H_2Y molecules. The charge densities at the BCPs were 0.0275−0.0260 and 0.0160−0.0145 au for *p*-CR·H_2O and *p*-CR·H_2S, respectively, at all three levels of calculations. These values of electron density and its Laplacian are well within the range specified for the existence

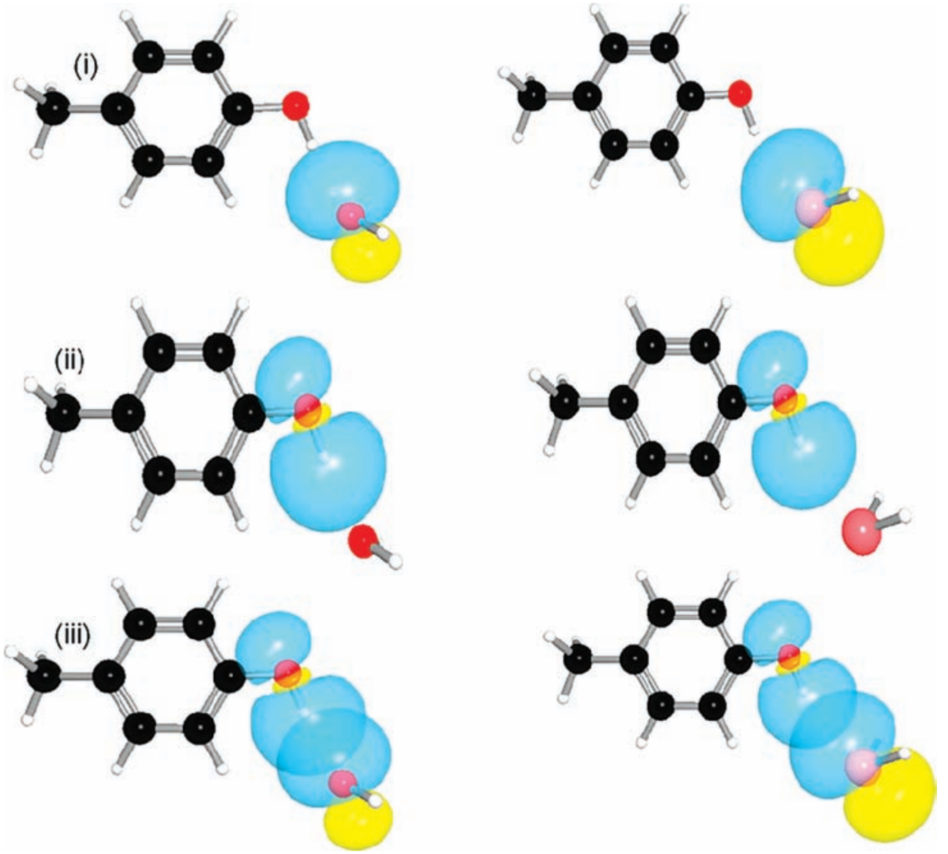

Figure 7. The interacting donor−acceptor natural bond orbitals (NBOs) ($n_{pY} \rightarrow \sigma^*_{O-H}$) of the *p*-CR·$H_2O$ (on the left) and *p*-CR·H_2S (on the right) complexes; (i) donor NBO (n_{pY}), (ii) acceptor NBO (σ^*_{O-H}), and (iii) donor−acceptor interacting NBOs ($n_{pY} \rightarrow \sigma^*_{O-H}$), where Y is either O or S.

of the hydrogen bond in terms of electron density (0.002−0.040 au) and its Laplacian (0.024−0.139 au).[66,67,69] In addition, Figure 6 also shows BCPs along the CH···Y bond paths, which were obtained using the MP2 wave functions only for both the complexes. The B3LYP and MPWB1K wave functions do not give these two BCPs. The values of the charge densities and the Laplacians at these two BCPs are an order of magnitude smaller than those for the BCPs between the OH···Y bond paths and hence can be safely ignored. The charge density at the BCP for the O−H···S interaction is significantly less than that for the O−H···O interaction. The Laplacian of charge density at the BCP was also smaller for the O−H···S interaction than that for the O−H···O interaction (see Table 5). The loss of electronic charge on the hydrogen atom for O−H···O hydrogen bonding was almost four times that of the O−H···S hydrogen bonding (the MP2 values from Table 5). The hydrogen atom in the *p*-CR·H_2O complex was destabilized almost two times that in the *p*-CR·H_2S complex, which clearly suggests that O−H···O hydrogen bonding is much stronger than the O−H···S hydrogen bonding. A similar trend was also observed for the decrease of dipolar polarization and the volume of the hydrogen atom.

5.3. Natural Bond Orbital (NBO) Analysis.

The NBO model has been very useful in explaining the hydrogen bonding in the X−H···Y system as the donor−acceptor charge delocalization takes place between the lone pair of the hydrogen bond acceptor Y and the proximal antibonding σ^*(X−H) orbital of the donor.[42−44,70] The NBO calculations were carried out for the complexes and monomers optimized at all three levels of theory. Table 6 lists the changes in the atomic charges on H [Δq(H)] and O or S (Δq(Y)) atoms, the occupancy in the lone pair orbital [$\delta(n_Y)$] and the antibonding orbital [$\delta(\sigma^*_{O-H})$], and the second-order perturbative interactions in the *p*-CR·H_2O and *p*-CR·H_2S complexes. In all cases, charge reduction on the H atom and an increase in the occupancy in the σ^*_{O-H} orbital were larger for the *p*-CR·H_2O complex than the *p*-CR·H_2S complex. This shows that there is a greater overlap of the lone pair orbital and the OH antibonding orbital in the *p*-CR·H_2O complex. A similar trend is also reflected in the $E^{(2)}_{i\rightarrow j^*}$ (second-order perturbation energy) values and the $\langle \varphi_i^{(0)} | \hat{F}_{KS} | \varphi_{j^*}^{(0)} \rangle$ values. Table 7 compiles the coefficients of various relevant orbitals of the monomer and the complexes. In the H_2O complex, the donor OH bond is more polarized, which is evident from the increased s character in both the oxygen lone pair (LP) and the σ^*_{O-H} orbital (Table 7). In the monomer (H_2O and H_2S), oxygen LP and sulfur LP orbitals are pure p-type orbitals, but in the complexes, the acceptor oxygen LP orbital is sp^2 type, while the sulfur LP remains almost as a p-type orbital. The orbital overlaps are pictorially shown in Figure 7. Figure 7a shows the extent of overlap between the oxygen LP and σ^*_{O-H}, which is greater than that between the sulfur LP and σ^*_{O-H} overlap (Figure 7b). All of these observations suggest that the relative weakness of the hydrogen bond in the H_2S complex can be attributed to relatively poor overlap between the sulfur LP and σ^*_{O-H} orbitals.

5.4. Energy Decomposition Analysis.

Although the experimental results, i.e., shifts in the O−H stretch and the band origin, as well as the computational results show that the O−H···O hydrogen bonding is stronger than the O−H···S hydrogen bonding, it is not clear what type of interactions dominate in each of the two cases, that is, the O−H···O hydrogen bonding versus the O−H···S hydrogen bonding. To better understand the nature and extent of different forces contributing to the intermolecular attraction in these complexes, individual energy components [electrostatic (ES), polarization (PL), charge transfer (CT)] of the total interaction energy were obtained using the Kitaura and Morokuma (KM),[50] reduced vibrational space self-consistent field (RVS),[51] and natural energy decomposition analysis (NEDA)[42] procedures. The total interaction energy along with the individual components obtained using the aforementioned procedures at the HF/aug-cc-pVDZ level are graphically presented in Figure 8. The dispersion energy was calculated as the difference between the BSSE-corrected total interaction energy computed at the MP2 level and that computed using the KM, RVS, and NEDA procedures. In the case of *p*-CR·H_2O the ES, CT, and PL contributions are large, while for the *p*-CR·H_2S complex, the dispersion energy is substantially greater than all other energy contributions. Table 8 gives the MP2 energies, the total interaction energies obtained using the aforementioned decomposition schemes, and the dispersion (ΔE_{disp}) energy contribution to the total energy for the *p*-CR·H_2O and the *p*-CR·H_2S complexes. The dispersion energy contribution to the total interaction energy for *p*-CR·H_2S is about 70%, while that for *p*-CR·H_2O it is only 25%. The dispersion contribution in the case of *p*-CR·H_2S is even higher than that reported in the case of the *p*-CR.Me_2S complex,[26] where it was 40% of the total binding energy. Therefore, it can be concluded that O−H···O hydrogen bonding in *p*-CR·H_2O is largely electrostatic in nature, but the O−H···S hydrogen bonding in *p*-CR·H_2S is predominantly dispersive in nature.

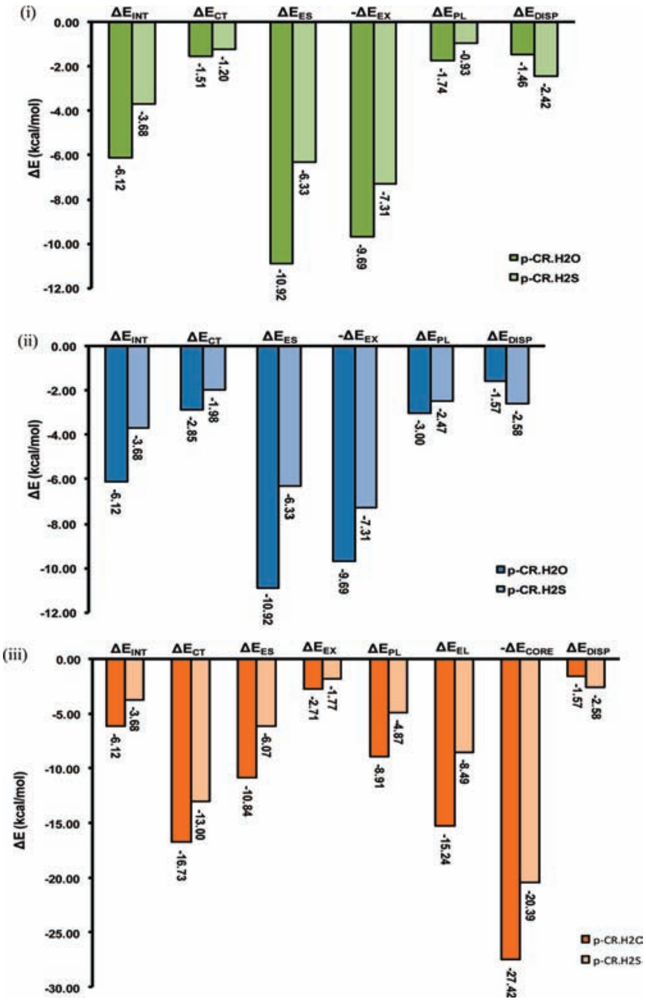

Figure 8. Decomposition of interaction energies of the *p*-CR·H_2O and *p*-CR·H_2S complexes using different energy decomposition schemes; (i) RVS, (ii) KM, and (iii) NEDA. ES = electrostatic term, PL = polarization term, EX = exchange repulsion, CT = charge transfer term, DEF = deformation term, SE = Slectrical self-energy term, and EL = the electrical contribution term. In NEDA scheme, $\Delta E_{\text{EL}} = \Delta E_{\text{ES}} + \Delta E_{\text{PL}} + \Delta E_{\text{SE}}$, $\Delta E_{\text{CORE}} = \Delta E_{\text{EX}} + \Delta E_{\text{DEF}} - \Delta E_{\text{SE}}$, and $\Delta E_{\text{INT}} = \Delta E_{\text{EL}} + \Delta E_{\text{CORE}} + \Delta E_{\text{CT}}$.

6. Discussion

Hydrogen-bonded complexes of common solvents such as H_2O, NH_3, and so forth with phenols and their derivatives have been widely studied over the last two decades. It has been established that in almost all cases, the phenol acts as the hydrogen bond donor. In the present context, the experimental data such as the shift in the S_1−S_0 band origin and the red shift in the phenolic OH stretching frequency in the case of the *p*-CR·H_2S complex suggest that the *p*-CR acts as the HB donor and the sulfur atom of H_2S acts as the acceptor. The magnitudes of the band origin shifts suggest that the relative stabilization of the S_1 state in the case of the H_2S complex (239 cm^{-1}) is much smaller than its H_2O counterpart (357 cm^{-1}). The intermolecular stretching frequency, σ, gives the direct measure of the strength of the H bond. The ratio of the mass-weighted stretching frequency of the H_2O complex to that of the H_2S complex for the ground state was 1.81, whereas that for the S_1 excited state was 1.66, which is consistent with the band origin shift data. The relative magnitudes of σ indicate that the OH···S HB in the *p*-CR·H_2S complex is almost half as strong as that in the OH···O HB in the *p*-CR·H_2O complex. Further, the relative increase in the HB strength in the excited state is smaller for the H_2S case compared to that in the H_2O complex. The other two modes, namely, 6a and 1, are almost unperturbed in the S_0 state as well as in the S_1 state for both complexes, suggesting that hydrogen bonding interaction with H_2O or H_2S has negligible influence on the force field for these two ring deformation modes.

The IR data on the OH stretching frequency of the parent monomer and its shift in the complex are very useful in determining the strength and nature of interaction. The OH frequency for the monomer was determined to be 3658 cm^{-1} in this work, and it was red shifted by 127 and 102 cm^{-1} in its H_2O and H_2S complexes, respectively. The IR red shift in the donor OH group has conventionally been taken as an indicator of the strength of the HB, and in that context, it can be inferred that the H_2S complex is weaker than the H_2O complex. However, there is a caveat. In the case of phenol, it has also been shown[71,72] that the OH red shift is well correlated with the proton affinity (PA) of the acceptor. The PA of H_2S is almost comparable or rather slightly higher than that of H_2O (168.7 versus 165.3 kcal/mol);[73] nevertheless, the OH red shift in the case of the H_2S complex is considerably smaller than that in the case of the H_2O complex. Therefore, it must be noted that although the IR shifts are consistent with other observations that suggest that the H_2S complex is weaker than the H_2O complex, it is not consistent with the acid−base formalism of the HB interactions. These observations indicate that the extent of electron transfer from the lone pair on the acceptor to the OH antibonding orbital is smaller in the case of the S atom as a HB acceptor, but it does not scale with the proton affinity of the acceptor, vide infra.

The phenol derivatives are known as photoacids, that is, in the excited state, they become strong acids (p$K_a \approx 3$), and the OH stretching frequency also red shifts considerably. For instance, in the case of phenol, the OH stretching frequency

TABLE 8: Total Interaction Energy (kcal/mol) at the MP2 Level ($\Delta E_{int}{}^{MP2}$), According to the NEDA, KM, and RVS Energy Decomposition Analyses (ΔE_{int}), and the Dispersion Energy (ΔE_{disp}) for the Two Complexes[a]

		ΔE_{int}			ΔE_{disp}		
complex	$\Delta E_{int}{}^{MP2}$	KM	RVS	NEDA	KM	RVS	NEDA
p-CR·H_2O	6.12	4.55	4.66	4.55	1.57 (26%)	1.46 (24%)	1.57 (26%)
p-CR·H_2S	3.68	1.10	1.26	1.10	2.58 (70%)	2.42 (66%)	2.58 (70%)

[a] Numbers in parentheses denote the percentage of contribution of the dispersion interaction to the total interaction energy.

shifts to 3581 from 3658 cm^{-1} in the ground state, indicating that the OH bond becomes weaker in the excited state, rendering it more labile for the proton transfer. It has been also shown that the OH stretch red shifts in the complexes are greater in the excited state relative to those in the ground state and show a linear correlation with the pK_a values. In the case of *p*-CR complexes, the red shift in the excited state of the H_2O complex was 188 cm^{-1}, whereas that in the case of H_2S complex was 152 cm^{-1}, compared to the red shifts of 127 and 102 cm^{-1} in their respective ground states. The increase in the red shift in the excited state relative to that in the ground state for both the H_2O and H_2S complexes is identical, that is, the ratio 188:127 is almost equal to 152:102. This indicates that the increase in the orbital interactions in the excited state is similar for both the O- and S-centered H bonds. However, the band origin shift and the intermolecular stretching frequency data suggest that in the case of the H_2S complex, the excited-state stabilization is smaller than that for the H_2O complex. Therefore, it is clear that the net interaction energy must consist of major contributions from forces other than electrostatic or charge-transfer energy.

The binding energy computed at the MP2 level for the H_2O and H_2S complexes was 4.29 and 2.29 kcal/mol, respectively. The energy computed using the MPWB1K functional is in excellent agreement with the MP2 value for the H_2O complex, which is consistent with the earlier reports.[35] The MPWB1K functional offers faster computation of the geometry-optimized structures and energies that are comparable to those obtained by employing the CCSD(T) levels for weak interactions. However, for the H_2S complex, the agreement was not so good; rather, it was found to be as poor as that computed at the B3LYP level. The MP2 binding energy values, with all its limitations,[27] are consistent with the trend observed in the intermolecular stretching frequencies (σ) for the two complexes and the observed relative red shifts of O−H stretch in RIDIRS spectra; the latter of the two is sort of related to the hydrogen bond strength.

The electron densities at the BCPs obtained using the AIM analyses were 0.0275−0.0260 and 0.0160−0.0145 au for *p*-CR·H_2O and *p*-CR·H_2S, respectively. The bond strength can be related to the magnitude of the charge density, and in that sense, these are consistent with the computed binding energies. The computation of the "the mutual penetration of hydrogen and the acceptor atom", that is, one of the AIM criteria for the existence of a hydrogen bond, is not so straightforward, and instead, the one proposed by Arunan et al.[74] was used in this work. They have reported the average donor bond radii, or the hydrogen bond radii (i.e., the distance between the BCP and the H atom), and the acceptor bond radii (the distance between the acceptor atom and the BCP) for a large number of acceptor molecules with a few H bond donors, which form strong, moderate, and weak hydrogen bonds. It was shown that the smaller the hydrogen bond radius, the stronger the hydrogen bond. The hydrogen bond radius of the *p*-CR donor computed in this work is smaller than the average $R_{H\cdots BCP}$ value ($\langle R_{H\cdots BCP}\rangle$) of the H_2O donor (Table 5), which is taken as a representative of the moderate H bond donors. This is consistent with the general experimental observation that *p*-CR is a stronger acid than water and does form strong hydrogen-bonded complexes with acceptors like water,[75] ammonia, and so forth. Extending this analogy further, it can be seen that the hydrogen bond radius in the case of *p*-CR·H_2O is smaller than that of *p*-CR·H_2S, suggesting that the latter complex is weaker than the former. This is well correlated with the experimentally observed shift in the O−H stretching frequencies. The acceptor bond radii ($R_{Y\cdots BCP}$) for H_2O and H_2S in the *p*-CR·H_2O and *p*-CR·H_2S are 1.25 and 1.70 Å, respectively, which matches very well with the average values $\langle R_{Y\cdots BCP}\rangle$ of 1.29 and 1.76 Å, respectively, reported in ref 74.

The detailed energy decomposition analysis has been very useful in bringing out the relative contributions of various types of interactions that exist in the weakly bound complexes. It was found that in the case of the *p*-CR·H_2S complex, the dispersion contribution to the total energy was as high as 70%. This information explains why the relative increase in the OH stretch red shifts in the excited state of the two complexes is identical although the relative stabilization of the S_1 state is substantially smaller in the case of the H_2S complex. It suggests that the smaller stabilization in the S_1 state of the H_2S complex relative to that of the H_2O complex must be due to the decrease in the dispersion contribution to the S_1 state of the former complex while all other contributions (read electrostatic interactions) that give rise to the OH stretch red shift must be comparable in both the complexes.

7. Conclusions

A detailed comparison between the HB complexes involving oxygen and sulfur acceptor atoms is reported for the first time with the help of both the experimental and computational studies. Experimental techniques like REMPI, SVLF, RIDIRS, and FDIRS were used to study the HB complexes of the *p*-CR·H_2O and *p*-CR·H_2S complexes in the jet-cooled condition. The red shift in the band origin for the *p*-CR·H_2S complex is much smaller compared to that of the *p*-CR·H_2O complex, which suggests that the relative stabilization of the S_1 state of the H_2S complex is smaller than that in the case of the H_2O complex. The intermolecular stretching frequencies (σ) in the S_0 and S_1 states of the H_2S complex are also smaller than those of H_2O complex (for the S_0 state, $\sigma_{H_2O}/\sigma_{H_2S} \sim 1.81$, and for the S_1 state, $\sigma_{H_2O}/\sigma_{H_2S} \sim 1.66$). This indicates that O−H···S HB strength in *p*-CR·H_2S is almost half of the O−H···O HB strength in the *p*-CR·H_2O complex. A similar trend was observed in the red shift of the O−H stretch for the two complexes with respect to the monomer O−H stretch. All experimental findings reveal that sulfur is not as good of a HB acceptor as oxygen.

The *ab initio* results show that O−H···S HB is much weaker than the O−H···O HB. The calculated interaction energy (at MP2/aug-cc-pVDZ) of the *p*-CR·H_2S complex (−2.49 kcal/

mol) was about 60% of the *p*-CR$\cdot$H$_2$O complex. The NBO analysis indicates that the orbital mixing upon complexation is quite different for the two complexes; that is, the lone pair on the S atom is pure p-type orbital, whereas in the case of the O atom, it is of sp^2 type. This results in the different orientations of the acceptor molecule with respect to the donor, that is, $\Psi \sim 90°$ for *p*-CR$\cdot$H$_2$S, whereas $\Psi \sim 135°$ for *p*-CR$\cdot$H$_2$O. The NBO analysis also indicates that the extent of overlap between the sulfur LP and $\sigma^*_{\mathrm{O-H}}$ is less compared to the oxygen LP and $\sigma^*_{\mathrm{O-H}}$ overlap, which in turn explains the smaller red shift of O$-$H stretch in the H$_2$S complex than that in the H$_2$O complex. All of the AIM criteria for HB also show that sulfur is a poor HB acceptor than oxygen. A detailed energy decomposition analysis reveals that the dispersion energy is the major contributor to the total interaction energy (~70%) of the O$-$H$\cdots$S HB *p*-CR$\cdot$H$_2$S complex. This is in contrast to the O$-$H$\cdots$O HB *p*-CR$\cdot$H$_2$O complex, where the dispersion energy contribution to the total interaction energy is only about 20%.

References and Notes

(1) (a) Jeffrey, G. A.; Saenger, W. *Hydrogen Bonding in Biological Structures*; Springer-Verlag: Berlin, Germany, 1991. (b) Jeffrey, G. A. *An Introduction to Hydrogen Bonding*; Oxford University Press: New York, 1997. (c) Scheiner, S. *Hydrogen Bonding: A Theoretical Perspective*; Oxford University Press: New York, 1997. (d) Desiraju, G. R.; Steiner, T. *The Weak Hydrogen Bond in Structural Chemistry and Biology*; Oxford University Press: New York, 1999. (e) Chalasinski, G.; Szczesniak, M. M. *Chem. Rev.* **2000**, *100*, 4227–4252. (f) Grabowski, S. J., Ed. *Hydrogen Bonding - New Insights*, 1st ed.; Springer: New York, 2006. (g) Hobza, P.; Zahradnik, R.; Muller-Dethlefs, K. *Collect. Czech. Chem. Commun.* **2006**, *71*, 443–531. (h) Cerny, J.; Hobza, P. *Phys. Chem. Chem. Phys.* **2007**, *9*, 5291–5303. (i) Buckingham, A. D.; Del Bene, J. E.; McDowell, S. A. C. *Chem. Phys. Lett.* **2008**, *463*, 1–10.

(2) Ratajcza, H *J. Phys. Chem.* **1972**, *76*, 3991–3992.

(3) Pauling, L. *J. Am. Chem. Soc.* **1932**, *54*, 3570–3582.

(4) Reid, K. S. C.; Lindley, P. F.; Thornton, J. M. *FEBS Lett.* **1985**, *190*, 209–213.

(5) Gregoret, L. M.; Rader, S. D.; Fletterick, R. J.; Cohen, F. E. *Proteins: Struct., Funct., Genet.* **1991**, *9*, 99–107.

(6) Pal, D.; Chakrabarti, P. *J. Biomol. Struct. Dyn.* **1998**, *15*, 1059–1072.

(7) Zauhar, R. J.; Colbert, C. L.; Morgan, R. S.; Welsh, W. J. *Biopolymers* **2000**, *53*, 233–248.

(8) Krepps, M. K.; Parkin, S.; Atwood, D. A. *Cryst. Growth Des.* **2001**, *1*, 291–297.

(9) Pal, D.; Chakrabarti, P. *J. Biomol. Struct. Dyn.* **2001**, *19*, 115–128.

(10) Hambley, T. W.; Hibbs, D. E.; Turner, P.; Howard, S. T.; Hursthouse, M. B. *J. Chem. Soc., Perkin Trans. 2* **2002**, 235–239.

(11) Iwaoka, M.; Takemoto, S.; Okada, M.; Tomoda, S. *Bull. Chem. Soc. Jpn.* **2002**, *75*, 1611–1625.

(12) Usman, A.; Fun, H. K.; Ganguly, N. C.; Datta, M.; Ghosh, K. *Acta Crystallogr., Sect. E* **2003**, *59*, O773−O775.

(13) Valdes-Martinez, J.; Hernandez-Ortega, S.; Rubio, M.; Li, D. T.; Swearingen, J. K.; Kaminsky, W.; Kelman, D. R.; West, D. X. *J. Chem. Crystallogr.* **2004**, *34*, 533–540.

(14) Ganguly, N. C.; Datta, M.; Ghosh, K.; Bond, A. D. *CrystEngComm* **2005**, *7*, 210–215.

(15) Ringer, A. L.; Senenko, A.; Sherrill, C. D. *Protein Sci.* **2007**, *16*, 2216–2223.

(16) Kim, K. S.; Tarakeshwar, P.; Lee, J. Y. *Chem. Rev.* **2000**, *100*, 4145–4185.

(17) Tsuzuki, S.; Honda, K.; Uchimaru, T.; Mikami, M.; Tanabe, K. *J. Am. Chem. Soc.* **2000**, *122*, 11450–11458.

(18) Arunan, E.; Emilsson, T.; Gutowsky, H. S.; Fraser, G. T.; de Oliveira, G.; Dykstra, C. E. *J. Chem. Phys.* **2002**, *117*, 9766–9776.

(19) Hermida-Ramon, J. M.; Cabaleiro-Lago, E. M.; Rodriguez-Otero, J. *J. Chem. Phys.* **2005**, *122*, 204315.

(20) Tauer, T. P.; Derrick, M. E.; Sherrill, C. D. *J. Phys. Chem. A* **2005**, *109*, 191–196.

(21) Wang, Y. X.; Paulus, B. *Chem. Phys. Lett.* **2007**, *441*, 187–193.

(22) Yan, S.; Lee, S. J.; Kang, S.; Choi, K. H.; Rhee, S. K.; Lee, J. Y. *Bull. Korean Chem. Soc.* **2007**, *28*, 959–964.

(23) Amicangelo, J. C.; Gung, B. W.; Irwin, D. G.; Romano, N. C. *Phys. Chem. Chem. Phys.* **2008**, *10*, 2695–2705.

(24) Cabaleiro-Lago, E. A.; Rodriguez-Otero, J.; Pena-Gallego, A. *J. Phys. Chem. A* **2008**, *112*, 6344–6350.

(25) Cabaleiro-Lago, E. M.; Rodriguez-Otero, J.; Pena-Gallego, A. *J. Chem. Phys.* **2008**, *129*, 084305−8.

(26) Biswal, H. S.; Chakraborty, S.; Wategaonkar, S. *J. Chem. Phys.* **2008**, *129*, 184311–7.

(27) Pauling, L. *J. Am. Chem. Soc.* **1931**, *53*, 1367–1400.

(28) Desiraju, G. R. *Acc. Chem. Res.* **2002**, *35*, 565–573.

(29) Howard, D. L.; Kjaergaard, H. G. *Phys. Chem. Chem. Phys.* **2008**, *10*, 4113–4118.

(30) Meenakshi, P. S.; Biswas, N.; Wategaonkar, S. *J. Chem. Phys.* **2002**, *117*, 11146–11151.

(31) Hobza, P.; Sponer, J. *Chem. Rev.* **1999**, *99*, 3247–3276.

(32) Shamovsky, I. L.; Riopelle, R. J.; Ross, G. M. *J. Phys. Chem. A* **2001**, *105*, 1061–1070.

(33) Bayari, S.; Saglam, S.; Ustundag, H. F. *J. Mol. Struct.: THEOCHEM* **2005**, *726*, 225–232.

(34) Zhang, R. B.; Somers, K. R. F.; Kryachko, E. S.; Nguyen, M. T.; Zeegers-Huyskens, T. S.; Ceulemans, A. *J. Phys. Chem. A* **2005**, *109*, 8028–8034.

(35) Zhao, Y.; Truhlar, D. G. *J. Chem. Theory Comput.* **2005**, *1*, 415–432.

(36) Frisch, M. J.; Trucks, G. W.; Schlegel, H. B.; Scuseria, G. E.; Robb, M. A.; Cheeseman, J. R.; Montgomery, J. A., Jr.; Vreven, T.; Kudin, K. N.; Burant, J. C.; Millam, J. M.; Iyengar, S. S.; Tomasi, J.; Barone, V.; Mennucci, B.; Cossi, M.; Scalmani, G.; Rega, N.; Petersson, G. A.; Nakatsuji, H.; Hada, M.; Ehara, M.; Toyota, K.; Fukuda, R.; Hasegawa, J.; Ishida, M.; Nakajima, T.; Honda, Y.; Kitao, O.; Nakai, H.; Klene, M.; Li, X.; Knox, J. E.; Hratchian, H. P.; Cross, J. B.; Bakken, V.; Adamo, C.; Jaramillo, J.; Gomperts, R.; Stratmann, R. E.; Yazyev, O.; Austin, A. J.; Cammi, R.; Pomelli, C.; Ochterski, J. W.; Ayala, P. Y.; Morokuma, K.; Voth, G. A.; Salvador, P.; Dannenberg, J. J.; Zakrzewski, V. G.; Dapprich, S.; Daniels, A. D.; Strain, M. C.; Farkas, O.; Malick, D. K.; Rabuck, A. D.; Raghavachari, K.; Foresman, J. B.; Ortiz, J. V.; Cui, Q.; Baboul, A. G.; Clifford, S.; Cioslowski, J.; Stefanov, B. B.; Liu, G.; Liashenko, A.; Piskorz, P.; Komaromi, I.; Martin, R. L.; Fox, D. J.; Keith, T.; Al-Laham, M. A.; Peng, C. Y.; Nanayakkara, A.; Challacombe, M.; Gill, P. M. W.; Johnson, B.; Chen, W.; Wong, M. W.; Gonzalez, C.; Pople, J. A. *Gaussian 03*, revision D.1; Gaussian, Inc.: Wallingford, CT, 2005.

(37) http://www.chemcraftprog.com.

(38) Bader, R. F. W. *Atoms in Molecules: A Quantum Theory*; Clarendon Press: Oxford, U.K., 1990.

(39) Bader, R. F. W. *Chem. Rev.* **1991**, *91*, 893–928.

(40) Bader, R. F. W. In *Encyclopedia of Computational Chemistry*; Schleyer, P. v. R., Allinger, N. L. T., Gasteiger Clark, J., Kollman, P. A., Schaefer, H. F. S., III, Schreiner, P. R., Eds.; Wiley: Chichester, U.K., 1998; Vol. 1, pp 64−86.

(41) AIM 2000 , Version 2; Bielefeld, Germany, 2002; www.aim2000.de.

(42) Weinhold, F. In *Encyclopedia of Computational Chemistry*; Schleyer, P. v. R., Allinger, N. L. T., Gasteiger Clark, J., Kollman, P. A., Schaefer III, H. F. S., III, Schreiner, P. R., Eds.; Wiley: Chichester, U.K., 1998; Vol. 3, pp 1792−1811.

(43) Weinhold, F.; Landis, C. R. *Chem. Educ. Res. Pract. Eur.* **2001**, *2*, 91–104.

(44) Weinhold, F.; Landis, C. R. *Valency and Bonding: A Natural Bond Orbital Donor-Acceptor Perspective*, Cambridge University Press: New York, 2005.

(45) Glendening, J., Badenhoop, K., Reed, A. E., Carpenter, J. E., Bohmann, J. A., Morales, C. M., Weinhold, F., Eds.; *NBO 5.0*; Theoretical Chemistry Institute, University of Wisconsin: Madison, WI, 2001.

(46) Chalasinski, G.; Szczesniak, M. M. *Chem. Rev.* **2000**, *100*, 4227–4252.

(47) Glendening, E. D.; Streitwieser, A. *J. Chem. Phys.* **1994**, *100*, 2900–2909.

(48) Glendening, E. D. *J. Am. Chem. Soc.* **1996**, *118*, 2473–2482.

(49) Schenter, G. K.; Glendening, E. D. *J. Phys. Chem.* **1996**, *100*, 17152–17156.

(50) Kitaura, K.; Morokuma, K. *Int. J. Quantum Chem.* **1976**, *10*, 325–340.

(51) Stevens, W. J.; Fink, W. H. *Chem. Phys. Lett.* **1987**, *139*, 15–22.

(52) Chen, W.; Gordon, M. S. *J. Phys. Chem.* **1996**, *100*, 14316–14328.

(53) Schmidt, M. W.; Baldridge, K. K.; Boatz, J. A.; Elbert, S. T.; Gordon, M. S.; Jensen, J. H.; Koseki, S.; Matsunaga, N.; Nguyen, K. A.; Su, S. J.; Windus, T. L.; Dupuis, M.; Montgomery, J. A. *J. Comput. Chem.* **1993**, *14*, 1347–1363.

(54) Lin, J. L.; Li, C. Y.; Tzeng, W. B. *J. Chem. Phys.* **2004**, *120*, 10513–10519.

(55) Tembreull, R.; Dunn, T. M.; Lubman, D. M. *Spectrochim. Acta, Part A* **1986**, *42*, 899–906.

(56) Pohl, M.; Schmitt, M.; Kleinermanns, K. *Chem. Phys. Lett.* **1991**, *177*, 252–260.

(57) Wolf, K.; Kuge, H. H.; Kleinermanns, K. *Z. Phys. D: At., Mol. Clusters* **1991**, *18*, 409–412.

(58) Ebata, T.; Ito, M. *J. Phys. Chem.* **1992**, *96*, 3224–3231.

(59) Fujimaki, E.; Fujii, A.; Ebata, T.; Mikami, N. *J. Chem. Phys.* **2000**, *112*, 137–148.

(60) Varsanyi, G. *Assignments of Vibrational Spectra of Seven Hundred Benzene Derivatives*; Wiley: New York, 1974.

(61) Bist, H. D; Brand, J. C. D.; Williams, D. R. *J. Mol. Spectrosc.* **1967**, *24*, 413-&.

(62) Ebata, T.; Mizuochi, N.; Watanabe, T.; Mikami, N. *J. Phys. Chem.* **1996**, *100*, 546–550.

(63) Tanabe, S.; Ebata, T.; Fujii, M.; Mikami, N. *Chem. Phys. Lett.* **1993**, *215*, 347–352.

(64) Watanabe, T.; Ebata, T.; Tanabe, S.; Mikami, N. *J. Chem. Phys.* **1996**, *105*, 408–419.

(65) Wennmohs, F.; Staemmler, V.; Schindler, M. *J. Chem. Phys.* **2003**, *119*, 3208–3218.

(66) Koch, U.; Popelier, P. L. A. *J. Phys. Chem.* **1995**, *99*, 9747–9754.

(67) Popelier, P. L. A. *J. Phys. Chem. A* **1998**, *102*, 1873–1878.

(68) Popelier, P. *Atoms In Molecules, An Introduction*; Prentice Hall: Englewood Cliffs, NJ, 2000.

(69) Grabowski, S. J. *J. Phys. Org. Chem.* **2004**, *17*, 18–31.

(70) Reed, A. E.; Curtiss, L. A.; Weinhold, F. *Chem. Rev.* **1988**, *88*, 899–926.

(71) Iwasaki, A.; Fujii, A.; Watanabe, T.; Ebata, T.; Mikami, N. *J. Phys. Chem.* **1996**, *100*, 16053–16057.

(72) Fujii, A.; Ebata, T.; Mikami, N. *J. Phys. Chem. A* **2002**, *106*, 8554–8560.

(73) Hunter, E. P. L.; Lias, S. G. *J. Phys. Chem. Ref. Data* **1998**, *27*, 413–656.

(74) Raghavendra, B.; Mandal, P. K.; Arunan, E. *Phys. Chem. Chem. Phys.* **2006**, *8*, 5276–5286.

(75) Page, R. H.; Frey, J. G.; Shen, Y. R.; Lee, Y. T. *Chem. Phys. Lett.* **1984**, *106*, 373–376.

JP9009355